catalysts

MDPI

Article

Exploring Long Range *para*-Phenyl Effects in Unsymmetrically Fused bis(imino)pyridine-Cobalt Ethylene Polymerization Catalysts

Yizhou Wang [1,2,†], Zheng Wang [1,3,†], Qiuyue Zhang [1], Song Zou [1], Yanping Ma [1], Gregory A. Solan [1,4,*], Wenjuan Zhang [1,5] and Wen-Hua Sun [1,2,*]

1 Key Laboratory of Engineering Plastics, Beijing National Laboratory for Molecular Sciences, Institute of Chemistry Chinese Academy of Sciences, Beijing 100190, China; wangyizhou13@iccas.ac.cn (Y.W.); wangzheng@iccas.ac.cn (Z.W.); zhangqiuyue@iccas.ac.cn (Q.Z.); zous22@iccas.ac.cn (S.Z.); myanping@iccas.ac.cn (Y.M.); zhangwj@bift.edu.cn (W.Z.)
2 CAS Research/Education Center for Excellence in Molecular Sciences and International School, University of Chinese Academy of Sciences, Beijing 100049, China
3 College of Science, Hebei Agricultural University, Baoding 071001, China
4 Department of Chemistry, University of Leicester, University Road, Leicester LE1 7RH, UK
5 Beijing Key Laboratory of Clothing Materials R&D and Assessment, Beijing Engineering Research Center of Textile Nanofiber, School of Materials Science and Engineering, Beijing Institute of Fashion Technology, Beijing 100029, China
* Correspondence: gas8@leicester.ac.uk (G.A.S.); whsun@iccas.ac.cn (W.-H.S.); Tel.: +44-(0)116-2522096 (G.A.S.); +86-10-6255-7955 (W.-H.S.)
† These authors contributed equally to this work.

Abstract: Unsymmetrical 11-phenyl-1,2,3,7,8,9,10-heptahydrocyclohepta[*b*]quinoline-4,6-dione, incorporating a *para*-phenyl substituted pyridine unit fused by both 6- and 7-membered carbocyclic rings, has been prepared on the gram-scale via a multi-step procedure involving cyclization, hydrogenation and oxidation. Templating this diketone, in the presence of cobalt(II) chloride hexahydrate, with the corresponding aniline afforded in good yield five examples of doubly fused bis(arylimino)pyridine-cobalt(II) chlorides, **Co1** (aryl = 2,6-dimethylphenyl), **Co2** (2,6-diethylphenyl), **Co3** (2,6-diisopropylphenyl), **Co4** (2,4,6-trimethylphenyl) and **Co5** (2,6-diethyl-4-methylphenyl). Structural characterization of **Co1**, **Co2** and **Co3** highlights the flexible nature of the inequivalent fused rings on the *NNN*′-ligand and the skewed disposition of the *para*-phenyl group. On activation with MAO, **Co1–Co5** exhibited high activity for ethylene polymerization at 30 °C (up to 5.66 × 10^6 g (PE) mol^{-1} (Co) h^{-1}) with the relative order being as follows: **Co4** > **Co1** > **Co5** > **Co3** > **Co2**. All polyethylenes were strictly linear, while their molecular weights and dispersities showed some notable variations. For **Co1**, **Co2**, **Co4** and **Co5**, all polymerizations were well controlled as evidenced by the narrow dispersities of their polymers (M_w/M_n range: 1.8–2.7), while their molecular weights (M_w range: 2.9–10.9 kg mol^{-1}) steadily increased in line with the greater steric properties of the *N*-aryl *ortho*-substituents. By contrast, the most hindered 2,6-diisopropyl counterpart **Co3** displayed a broad distribution with bimodal characteristics (M_w/M_n = 10.3) and gave noticeably higher molecular weight polymer (M_w = 75.5 kg mol^{-1}). By comparison, the MMAO-activated catalysts were generally less active, but showed similar trends in molecular weight and polymer dispersity. End group analysis of selected polymers via ^{13}C and ^{1}H NMR spectroscopy revealed the presence of both saturated and unsaturated polyethylenes in accordance with competing chain transfer pathways. Notably, when comparing **Co3**/MAO with its non-phenyl substituted analogue ($E_{2,6\text{-iPr2Ph}}$)$CoCl_2$/MAO, the former, though less controlled, displayed higher activity and molecular weight, a finding that points towards a role played by the remote *para*-phenyl group.

Keywords: cobalt catalysts; carbocyclic-fused *N,N,N* ligands; ethylene polymerization; substituent effects; high activity

Citation: Wang, Y.; Wang, Z.; Zhang, Q.; Zou, S.; Ma, Y.; Solan, G.A.; Zhang, W.; Sun, W.-H. Exploring Long Range *para*-Phenyl Effects in Unsymmetrically Fused bis(imino)pyridine-Cobalt Ethylene Polymerization Catalysts. *Catalysts* **2023**, *13*, 1387. https://doi.org/10.3390/catal13101387

Academic Editors: Marc Visseaux and Luca Gonsalvi

Received: 16 August 2023
Revised: 19 October 2023
Accepted: 20 October 2023
Published: 23 October 2023

1. Introduction

Ever since the first communications of molecular iron and cobalt complexes as catalysts for ethylene polymerization towards the end of the 1990s [1], numerous efforts have been devoted to modifying the supporting 2,6-bis(imino)pyridine ligand framework (**A**, Scheme 1) [1–3]. Indeed, the importance of structural variations to **A** was noted early in their development with catalysts able to mediate both ethylene polymerization and oligomerization [1–7]. In the intervening years, a wide variety of alternative *N,N,N* chelating ligands related to **A** have been disclosed [8–11], including 2-imino-1,10-phenanthrolines (**B**, Scheme 1) [12–16], 2,8-bis(imino)quinolines [17,18] and various other pyridine-containing derivatives [19,20]. Significantly, **B**-type iron catalysts have reached the pilot-scale for the production of linear α-olefins [12], a disclosure that underscores their value for large scale industrialization.

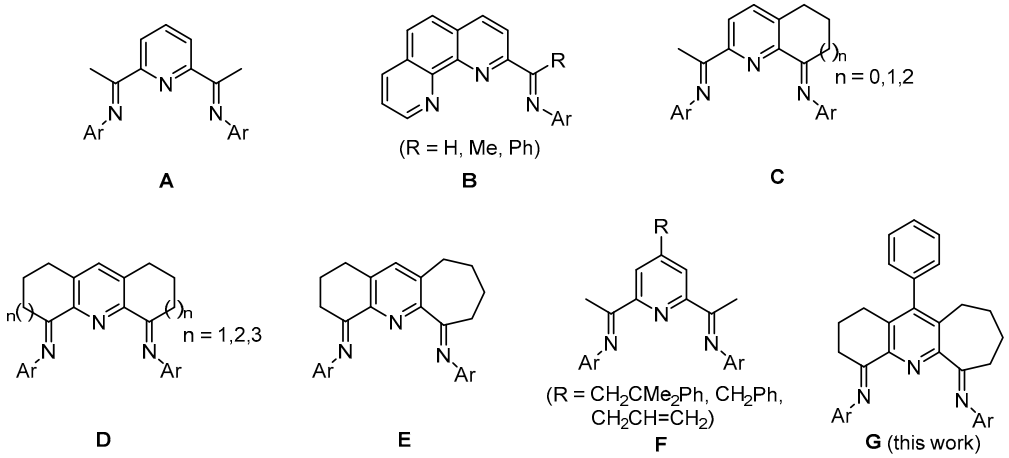

Scheme 1. Parent bis(arylimino)pyridine **A**, its relatives **B**–**F** and the subject of this work, **G**.

With regard to specific changes to the *N,N,N* ligand framework, most efforts have focused on varying the steric and electronic properties of the *N*-aryl substituents belonging to **A**, with an aim to enhance the thermal stability and increase the activity of their cobalt and iron catalysts [21–30]. More recently, considerable efforts have been directed towards the development of carbocyclic-fused bis(imino)pyridine ligands, as the size of the fused ring can affect the catalyst performance and product type (e.g., **C** [17,18,31–33] and **D** [34–36], Scheme 1). For example, cobalt catalysts bearing the doubly fused six-membered ring $\mathbf{D}_{6,6}$ (n = 1, Scheme 1) [34] produced mixtures of linear α-olefins and polyethylene waxes in a good yield, while those involving the seven-membered ring counterpart $\mathbf{D}_{7,7}$ (n = 2, Scheme 1) [35] afforded linear polyethylene of low molecular weight with relatively narrow dispersity. On the other hand, for the larger and more flexible eight-membered ring $\mathbf{D}_{8,8}$ (n = 3, Scheme 1), their cobalt catalysts [36] generated high molecular weight linear polyethylene of narrow dispersity. On account of this marked effect of the fused ring size, the mixed ring cobalt complex $\mathbf{E}_{6,7}$ (Scheme 1) containing both six- and seven-membered carbocycles has also been explored [37]. Indeed, this class of unsymmetrical cobalt catalysts proved highly active, generating highly linear vinyl-terminated polyethylene with low molecular weights and extremely narrow dispersity when activated with MAO, while with MMAO, fully saturated polymers were detected.

Elsewhere, the functionalization of bis(imino)pyridine-cobalt or -iron complexes at the *para*-position of the central pyridine with alkyl or allyl groups have been reported (**F**, Scheme 1). Notably, this *para*-substitution had little effect on the activity of the catalyst but does have an effect on chain propagation with higher molecular weight polymers with broader dispersity generated for the allyl derivative. The origin of this behavior was uncertain but was tentatively attributed to a self-immobilization phenomenon [38].

Given the effect on catalyst performance and polymer properties caused by (i) ring size variations in **D** and **E** and (ii) the *para*-substituents to the central pyridine in **F**, we decided

to target a carbocyclic-fused bis(imino)pyridine-cobalt catalyst *para*-functionalized with a phenyl group. We reasoned that the inclination of this aromatic group could potentially affect the flexibility of the neighboring carbocycles and, in turn, the steric protection of the metal center imparted by the *N*-aryl groups. Alternatively, the electronic properties of the *para*-phenyl group could influence the electropositivity of the active species as well as increase the solubility of the catalyst. To this end, we target five cobalt examples of **G** (Scheme 1) in which the steric and electronic properties of the two *N*-aryl groups are systematically varied. A thorough polymerization investigation is then undertaken using (**G**)$CoCl_2$ that makes use of two different aluminoxane activators with the aim to identify trends in catalyst performance and to compare these findings with their non-phenyl substituted counterpart (**E**)$CoCl_2$ [37]. Besides the polymerization study, full synthetic details for the cobalt complexes as well as the diketone precursor are presented.

2. Results

*2.1. Synthesis and Characterization of **Co1–Co5***

The 4,6-bis(arylimino)-11-phenyl-1,2,3,7,8,9,10-heptahydrocyclohepta[*b*]quinoline-cobalt (II) chlorides, **Co1** (aryl = 2,6-dimethylphenyl), **Co2** (2,6-diethylphenyl), **Co3** (2,6-diisopropylphenyl), **Co4** (2,4,6-trimethylphenyl) and **Co5** (2,6-diethyl-4-methylphenyl), were obtained in good yield (62–81%) via a one-pot route, whereby 11-phenyl-1,2,3,7,8,9,10-heptahydrocyclohepta[*b*]quinoline-4,6-dione (**3**) was treated with four equivalents of the corresponding aniline and $CoCl_2 \cdot 6H_2O$ in *n*-butanol at reflux with acetic acid utilized as catalyst (Scheme 2). For **Co1**, a similar one-pot route was also conducted in acetic acid as solvent, though the yield of the isolated complex was lower (*ca.* 24%). All attempts to prepare the free 4,6-bis(arylimino)-11-phenyl-1,2,3,7,8,9,10-heptahydrocyclohepta[*b*]quinolines via the condensation of **3** with the corresponding aniline proved unsuccessful [24,26,39]. Complexes **Co1**–**Co5** were characterized via microanalysis, FT-IR spectroscopy and, in the cases of **Co1**, **Co2** and **Co3**, with single crystal X-ray diffraction.

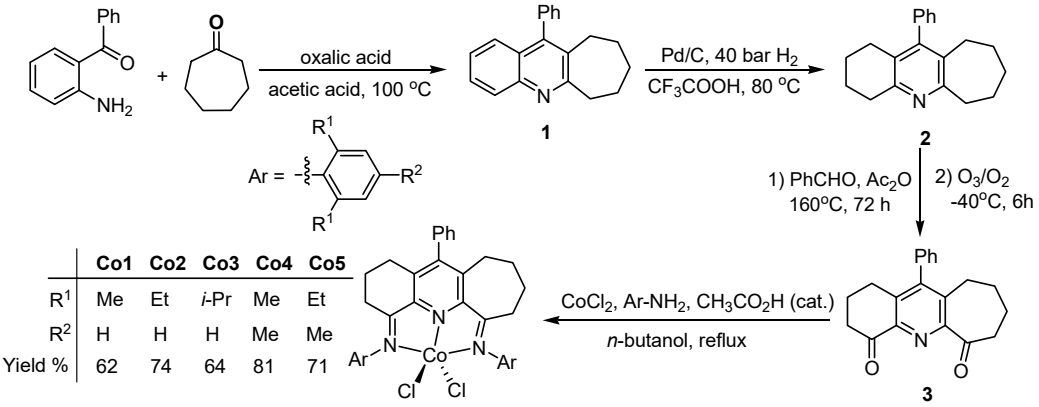

Scheme 2. One-pot synthesis of **Co1**–**Co5** including the stepwise route to diketone precursor **3.**

The diketone itself, **3**, was obtained using a multi-step procedure (Scheme 2). Initially, a Friedlander condensation reaction of 2-aminobenzophenone with cycloheptanone in acetic acid, in the presence of oxalic acid, gave 11-phenyl-6,7,8,9,10-pentahydrocyclohepta[*b*]quinoline (**1**) [40–42], which could then be hydrogenated with 10% Pd/C in trifluoroacetic acid to form 11-phenyl-1,2,3,4,6,7,8,9,10-nonahydrocyclohepta[*b*]quinoline (**2**) [43,44]. Compound **3** was then accessed in two steps, involving firstly a dehydration condensation reaction of **2** with benzaldehyde and then oxidation of the resulting intermediate with ozone/oxygen [43,45]. Compounds **1**–**3** were characterized using ^{1}H NMR and ^{13}C NMR spectroscopy (see experimental).

Single crystals of **Co1**, **Co2** and **Co3**, suitable for the X-ray determinations, were grown via the slow diffusion of diethyl ether into dichloromethane solutions of the respective

complex at ambient temperature. Views of **Co1**, **Co2** and **Co3** are depicted in Figures 1–3, while selected bond distances and angles are given in Table 1.

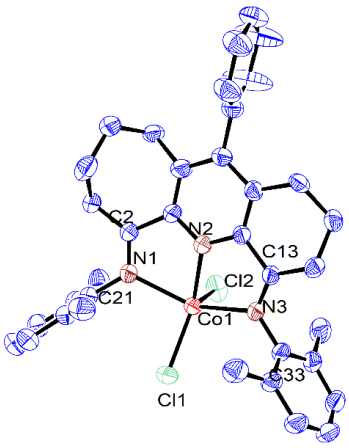

Figure 1. ORTEP representation of **Co1** with the thermal ellipsoids shown at the 50% probability level; all the hydrogen atoms have been omitted for clarity.

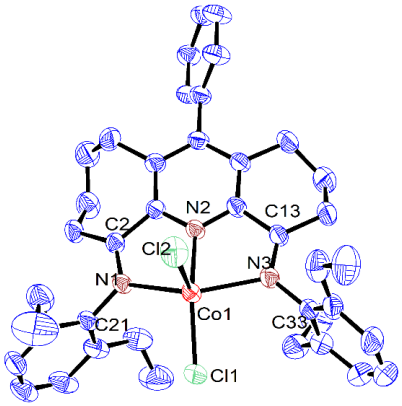

Figure 2. ORTEP representation of **Co2** with the thermal ellipsoids shown at the 50% probability level; all the hydrogen atoms and the dichloromethane have been omitted for clarity.

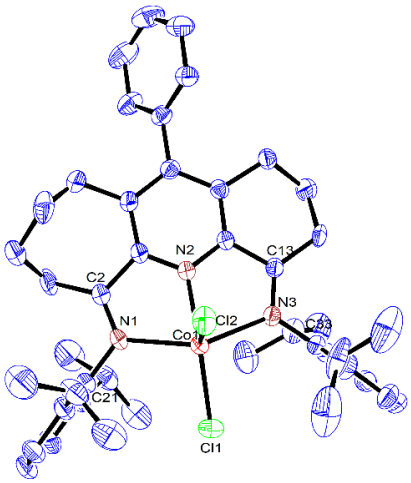

Figure 3. ORTEP representation of **Co3** with the thermal ellipsoids shown at the 50% probability level; all the hydrogen atoms have been omitted for clarity.

Table 1. Selected bond lengths and angles for **Co1**, **Co2** and **Co3**.

	Co1	**Co2**	**Co3**
		Bond lengths (Å)	
Co(1)-N(2)	2.056(2)	2.050(2)	2.0616(19)
Co(1)-N(1)	2.202(2)	2.195(2)	2.1600(18)
Co(1)-N(3)	2.183(2)	2.221(2)	2.2211(18)
Co(1)-Cl(1)	2.2427(7)	2.2450(8)	2.2471(7)
Co(1)-Cl(2)	2.2967(8)	2.2824(9)	2.3043(7)
N(1)-C(2)	1.276(3)	1.286(4)	1.278(3)
N(1)-C(21)	1.432(3)	1.445(3)	1.441(3)
N(3)-C(13)	1.281(3)	1.285(4)	1.284(3)
N(3)-C(33)	1.435(3)	1.435(4)	1.442(3)
		Bond angles (°)	
Cl(1)-Co(1)-Cl(2)	114.01(3)	118.71(4)	115.15(3)
N(2)-Co(1)-Cl(1)	149.05(7)	149.63(7)	154.97(6)
N(2)-Co(1)-Cl(2)	96.77(7)	91.66(7)	89.88(6)
N(1)-Co(1)-Cl(1)	96.31(6)	99.17(6)	99.78(6)
N(1)-Co(1)-Cl(2)	101.06(6)	98.98(7)	101.07(6)
N(3)-Co(1)-Cl(1)	101.36(6)	97.96(7)	99.14(5)
N(3)-Co(1)-Cl(2)	100.83(6)	101.20(7)	101.96(5)
N(3)-Co(1)-N(1)	143.14(8)	142.88(9)	140.24(8)
N(2)-Co(1)-N(1)	73.62(8)	74.23(9)	74.188(7)
N(2)-Co(1)-N(3)	74.64(8)	74.36(9)	73.92(7)

As has been noted previously [37], positional disorder can be a feature of mixed fused-ring complexes, and indeed in **Co1** and **Co3**, the six- and seven-membered carbocyclic rings are disordered across both positions. Each structure was composed of a single cobalt center coordinated by a *N,N,N*′-coordinated 4,6-bis(arylimino)-11-phenyl-1,2,3,7,8,9,10-heptahydrocyclohepta[*b*]quinoline (aryl = 2,6-dimethylphenyl **Co1**, 2,6-diethylphenyl **Co2**, 2,6-diisopropylphenyl **Co3**) and two chloride ligands to complete a five-coordinate geometry that can be best viewed as distorted square-based pyramidal with three nitrogen atoms and Cl1 forming the base and Cl2 the apex. By using the tau value (where $\tau = 1$ is an ideal trigonal bipyramid and $\tau = 0$ an ideal square pyramidal), some degree of quantification of the distortion can be given [46]. For these three structures, $\tau = 0.10$ (**Co1**), 0.11 (**Co2**) and 0.24 (**Co3**) (calculated using the equation $(\beta-\alpha)/60$, where β and α are the two largest angles, $\beta > \alpha$) which indicates some modest variation in the distortion from the idealized square-based pyramidal. The cobalt atom itself sits above the basal plane (defined by N1-N2-N3-Cl1) by 0.478 Å (**Co1**), 0.506 Å (**Co2**) and 0.593 Å (**Co3**), which resembles that seen in a number of their cobalt analogues [37]. Of the three cobalt–nitrogen distances, that involving the central pyridine (Co1-N2) displays the shortest bond length of 2.052(2) Å (**Co1**), 2.050(2) Å (**Co2**) and 2.062(2) Å (**Co3**) on account of the stronger coordination between N_{py} and the cobalt center. By comparison, the longer bond lengths involving the exterior nitrogen atoms show some dissimilarity with that involving N3 (6-membered ring) longer than for N1 (7-membered ring) for **Co2** and **Co3** (Co1-N3 2.221(2) Å (**Co2**), 2.221(2) Å (**Co3**) vs. Co1-N1 2.195(2) Å (**Co2**), 2.160(2) Å (**Co3**)), whereas the converse is true for **Co1** (Co1-N3 2.183(2) Å vs. Co1-N1 2.202(2) Å (**Co1**). When the structure of **Co3** is related to its non-phenyl substituted comparator ($\mathbf{E}_{2,6\text{-iPr2Ph}}$)$CoCl_2$ (Scheme 1) [37], the variation in the Co-N3 and Co-N1 distances for the latter are considerably less pronounced, while the Co1-N2 distance is slightly shorter (2.040(1) vs. 2.062(2) Å **Co3**). Hence, it is evident the *para*-phenyl group on the central pyridine has some effect on the binding properties of the *N,N,N*′ chelating ligand in **Co3**. In terms of the *N,N,N*′ coordination plane in **Co1**–**Co3**, some minor deviation from coplanarity is observed between the pyridine and imine groups as is evidenced by the torsion angles of N1-C2-C1-N2 (4.604° **Co1**, 9.950° **Co2**, 4.616° **Co3**) and N2-C14-C13-N3 (8.022° **Co1**, 2.906° **Co2**, 5.692° **Co3**). As expected, the saturated sections of the six- and seven-membered carbocycles adopt puckered arrangements, with

the latter showing the most flexibility. With respect to the *para*-phenyl group, there is some dissimilarity in the inclination of the phenyl group with respect to the adjacent pyridine plane (torsion angle: 79.8° **Co1**, 66.1° **Co2**, 54.8° **Co3**), which highlights the rotational flexibility of this unit. As is common, the *N*-aryl rings are inclined close to perpendicular with respect to the *N*,*N*,*N* coordination planes in all three cobalt structures [37]. There were no obvious intermolecular interactions in each structure.

In the IR spectra of **Co1**–**Co5**, characteristic absorption peaks for the imine double bonds are seen at around 1620 cm^{-1}, which correspond to values of wavenumber typically seen for coordinated imines in related cobalt complexes [35–37,39]. In addition, their microanalytical data for all five complexes support compositions of the type $LCoCl_2$.

2.2. Ethylene Polymerization Studies

In previous studies involving *N*,*N*,*N*-cobalt(II) halide complexes such as **A**–**F** (Scheme 1), high productivity for ethylene polymerization has been achieved when these precatalysts were pretreated with either MAO (methylaluminoxane) or MMAO (modified MAO) [8,9,18,34–38,47–49]. From a previous study [2], the **Co3** precatalyst was the most steric hindered one in the set, which was thought of as a highly soluble and thermostable precatalyst that could obtain a higher molecular weight polymer. To magnify the advantage of the catalytic system in this work, **Co3** was chosen to screen the polymerization conditions. Consequently, this work employs both of these aluminoxanes as part of two parallel studies concerned with exploring both their effectiveness as activators for **Co1**–**Co5** and also their influence on the properties of the polymers produced. All runs were conducted in toluene in a stainless-steel reactor (P_{C2H4} = 5 or 10 atm) or Schlenk vessel (P_{C2H4} = 1 atm) with the ethylene pressure initially set at 10 atm.

2.2.1. Ethylene Polymerization Evaluation Using **Co1**–**Co5** with MAO as Activator

With MAO initially employed as the aluminoxane, we set about determining an effective set of operating conditions for the polymerizations by using **Co3** as our test precatalyst. As part of this preliminary optimization, we systematically examine the effects of the activator to precatalyst ratio (i.e., Al:Co molar ratio), run temperature, reaction time and the pressure of ethylene; the complete set of results are given in Table 2.

Table 2. Ethylene polymerization evaluation using **Co1**–**Co5** with MAO as activator [a].

Entry	Precat.	Al:Co	T (°C)	t (min)	Activity [b]	M_w [c]	M_w/M_n [c]	T_m (°C) [d]
1	**Co3**	2500	30	30	3.57	65.6	10.7	133.0
2	**Co3**	3000	30	30	3.62	70.8	10.9	131.9
3	**Co3**	3500	30	30	3.95	72.4	10.5	131.6
4	**Co3**	4000	30	30	4.18	75.5	10.3	132.1
5	**Co3**	4500	30	30	4.07	82.6	11.6	132.0
6	**Co3**	5000	30	30	3.65	73.9	11.6	132.2
7	**Co3**	4000	20	30	3.95	85.4	12.3	133.2
8	**Co3**	4000	40	30	2.70	45.6	8.6	132.3
9	**Co3**	4000	50	30	2.35	35.5	7.6	131.4
10	**Co3**	4000	60	30	1.75	32.7	5.7	131.3
11	**Co3**	4000	30	5	8.10	77.6	10.0	132.3
12	**Co3**	4000	30	15	7.36	77.5	9.1	131.8
13	**Co3**	4000	30	45	2.93	78.4	8.8	131.4
14	**Co3**	4000	30	60	2.44	77.5	9.6	131.4
15 [e]	**Co3**	4000	30	30	0.60	56.3	6.9	131.6
16 [f]	**Co3**	4000	30	30	2.82	70.3	10.8	131.6
17	**Co1**	4000	30	30	4.40	3.4	2.2	123.8
18	**Co2**	4000	30	30	3.50	9.4	1.8	129.8
19	**Co4**	4000	30	30	5.66	2.9	2.0	122.7
20	**Co5**	4000	30	30	4.60	10.9	2.7	128.3

[a] General conditions: 2.0 µmol of the cobalt precatalyst, MAO as activator, 100 mL of toluene, 10 atm of ethylene; [b] Values in units of 10^6 g (PE) mol^{-1} (Co) h^{-1}; [c] M_w and M_n in units of kg mol^{-1}, determined via GPC; [d] Determined via DSC; [e] 1 atm of ethylene and 30 mL of toluene; [f] 5 atm of ethylene.

In view of the key role played by the aluminoxane activator, we first looked at determining the optimal Al:Co molar ratio using **Co3**/MAO. Accordingly, this was adjusted from 2500:1 to 5000:1 with the reaction temperature kept at 30 °C and the resulting level of catalytic activity monitored (entries 1–6, Table 2). The highest value of 4.18 × 10^6 g (PE) mol^{-1} (Co) h^{-1} was obtained with the ratio at 4000:1 (Table 2). Nonetheless, good activity was also realized with the Al:Co molar ratio at 2500:1 (3.57 × 10^6 g (PE) mol^{-1} (Co) h^{-1}) (entry 1, Table 2) or 5000:1 (3.65 × 10^6 g (PE) mol^{-1} (Co) h^{-1}) (entry 6, Table 2), reflecting the broad range in Al:Co molar ratios that can sustain high activity.

With regard to the polyethylenes generated using the different molar ratios, broad dispersities (M_w/M_n range: 10.3–11.6) were a feature with clear evidence of bimodality seen in their GPC traces (Figure 4). In terms of their molecular weights, these fell in the range 65.6 to 82.6 kg mol^{-1}, with a ratio of 4500:1 yielding the highest molecular weight polymer. Interestingly, at ratios in excess of 4500:1, the molecular weight starts to decrease as chain transfer from the active cobalt species to MAO (or $AlMe_3$) likely becomes more prominent [35].

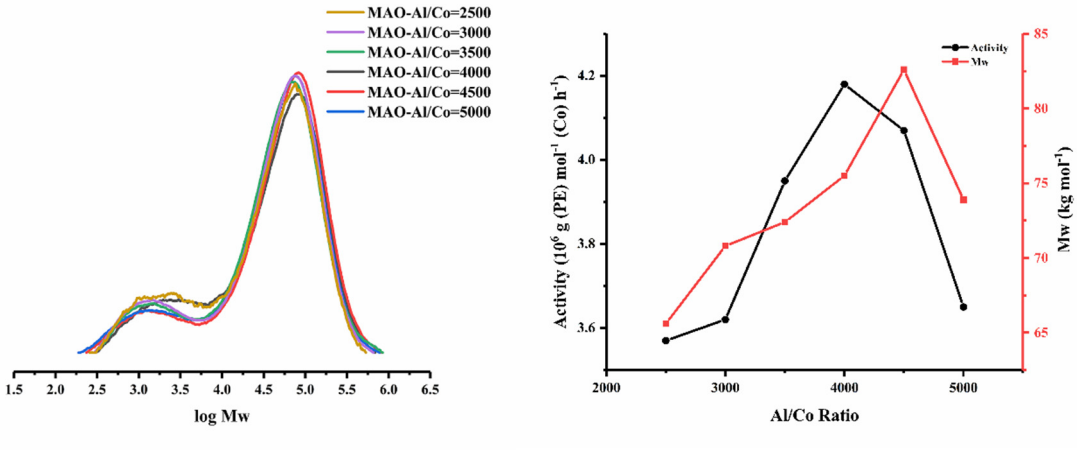

(**a**) (**b**)

Figure 4. (**a**) GPC traces for the polymers obtained using **Co3**/MAO at various Al:Co molar ratios and (**b**) plots of catalytic activity and polymer M_w as a function of the Al:Co molar ratio.

Next, with the Al:Co molar ratio maintained at 4000:1, the run temperature using **Co3**/MAO was varied between 20 °C and 60 °C (entries 4, and 7–10, Table 2). With the temperature at 30 °C, the highest activity of 4.18 × 10^6 g (PE) mol^{-1} (Co) h^{-1} was recorded, which compares to 40 °C seen for its non-phenyl containing comparator ($\mathbf{E}_{2,6\text{-iPr2Ph}}$)$CoCl_2$ (Scheme 1). As the temperature increased beyond 30 °C, the activity steadily lowered, reaching a minimum of 1.75 × 10^6 g (PE) mol^{-1} (Co) h^{-1} at 60 °C. Such a decline in performance may be due to the lower solubility of ethylene at higher temperatures [50], while partial deactivation of the active species may provide another possible contributing factor [2]. As for the molecular weight of the polymer, this gradually descended as the temperature increased from 85.4 kg mol^{-1} at 20 °C to 32.7 kg mol^{-1} at 60 °C (Figure 5) on account of the greater rate of chain transfer occurring [35]. Moreover, the dispersity narrowed (M_w/M_n: from 12.3 to 5.7) as the temperature was raised, while the bimodal feature became less pronounced. Although uncertain, the broad dispersity could plausibly originate from the multiple active centers of **Co3** [27], whereby the phenyl group could adopt either a more coplanar or a more orthogonal conformation with respect to the pyridine unit, leading to variations in the flexibility of the neighboring fused carbocycles and the inclination of the *N*-2,6-diisopropylphenyl group. In turn these structural differences could impact on the number of active species and/or chain transfer pathways (e.g., chain transfer to aluminum or β-H elimination to metal or monomer [51–56]). Based on this proposal, the

higher temperature would conceivably drive the favored conformation of the phenyl group to give to a more uniform active species or promote a single chain transfer pathway.

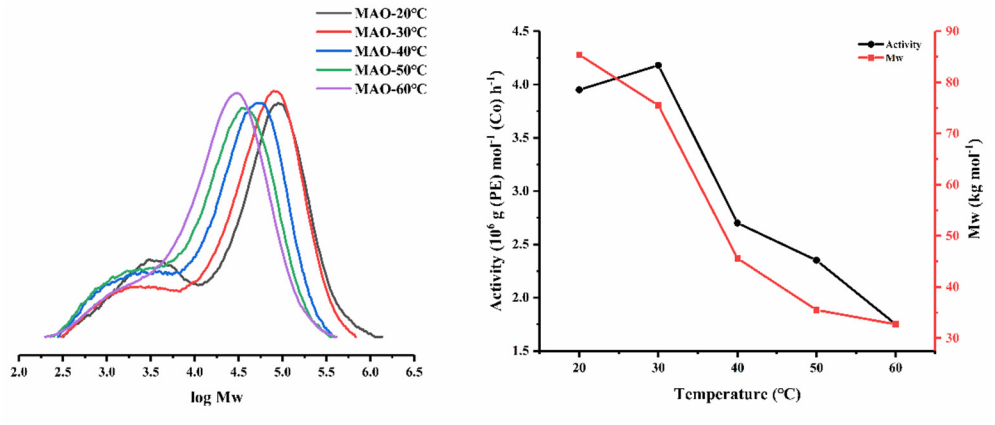

(**a**) (**b**)

Figure 5. (**a**) GPC traces for the polymers acquired using **Co3**/MAO at various temperatures and (**b**) plots of catalytic activity and polymer M_w as a function of reaction temperature.

To look into the performance of **Co3**/MAO over time, the polymerizations were performed at set times of 5, 15, 30, 45 and 60 min with the Al:Co molar ratio at 4000:1 and the temperature fixed at 30 °C (entries 4 and 11–14, Table 2). The maximum activity of 8.10×10^6 g (PE) mol^{-1} (Co) h^{-1} was achieved after a 5 min run time (entry 11, Table 2), which then reduced by more than three times after 1 h, culminating in a level of 2.44×10^6 g (PE) mol^{-1} (Co) h^{-1} (Figure 6). Evidently, the active species was rapidly generated following the addition of MAO and then was able to sustain a reasonably constant level of performance as time elapsed, a finding that reflects its good lifetime [35]. On the other hand, the molecular weight of the polymer remained essentially constant over time [M_w range: 75.5–78.4 kg mol^{-1}].

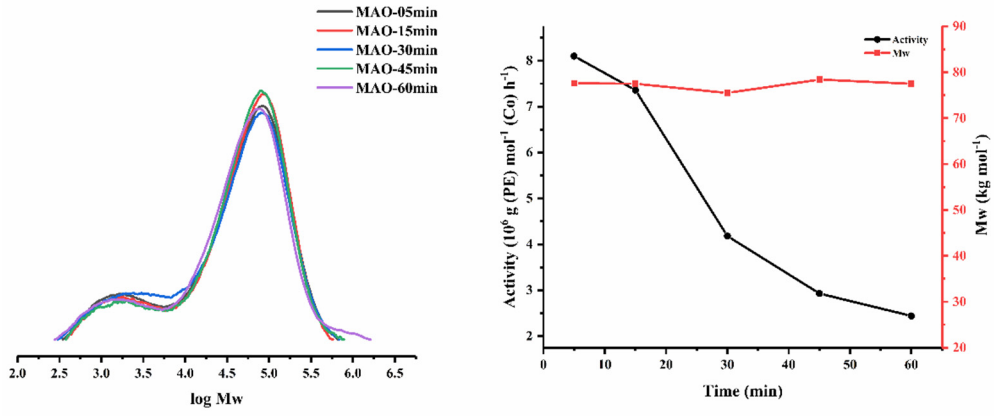

(**a**) (**b**)

Figure 6. (**a**) GPC traces for the polymers acquired using **Co3**/MAO at various reaction times and (**b**) plots of its catalytic activity and polymer M_w as a function of the reaction time.

To explore the influence of ethylene pressure on the performance of **Co3**/MAO, this parameter was initially lowered to 5 atm and then 1 atm with the conditions otherwise identical. At 5 atm, the catalytic activity decreased by approximately half while the molecular weight was slightly lowered (entry 16, Table 2). On the other hand, at 1 atm of ethylene pressure, the polymerization activity dropped more dramatically to 0.60×10^6 g (PE) mol^{-1} (Co) h^{-1} while the molecular weight was lowered to 56.3 kg mol^{-1} (entry 15, Table 2).

Hence, it is apparent that higher ethylene pressure not only promotes higher molecular weight polymer but also higher activity, which can be attributed to the higher concentration of ethylene gas in the reaction system [37].

Finally, the remaining cobalt complexes, **Co1**, **Co2**, **Co4** and **Co5**, were screened in combination with MAO using the optimized conditions established for **Co1** (Al:Co molar ratio, 4000:1; temp., 30 °C; P_{C2H4}, 10 atm) (entries 17–20, Table 2). Examination of the data reveals that all these precatalysts, including **Co3**, displayed high activity in the range 3.50 to 5.66 × 10^6 g (PE) mol^{-1} (Co) h^{-1}, with the relative level being **Co4** (2,4,6-trimethyl) > **Co5** (2,6-diethyl-4-methyl) > **Co1** (2,6-dimethyl) > **Co3** (2,6-diisopropyl) > **Co2** (2,6-diethyl) (Figure 7). Analysis of this order would suggest that both steric and electronic properties are influential. Notably, *para*-methyl **Co4** and **Co5** showed a higher activity than their *para*-H comparators, implying that the electron-donating properties of this substituent were beneficial; the improved solubility could also be a supporting factor [35–37]. Moreover, **Co4** displayed a superior activity to **Co5**, indicating that the bulkier *ortho* groups have an unfavorable effect on catalytic activity [37].

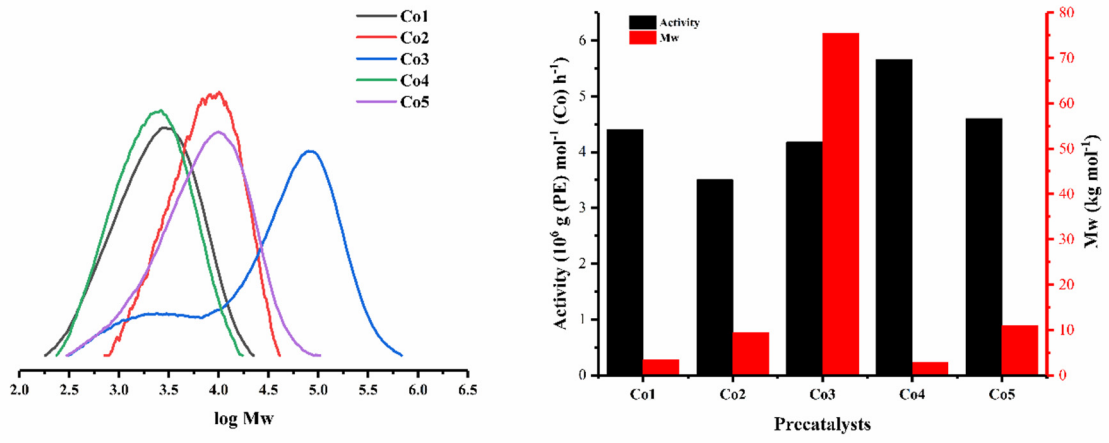

(**a**) (**b**)

Figure 7. (**a**) GPC traces for the polymers produced using **Co1**–**Co5** with MAO as activator and (**b**) a bar chart showing their relative catalytic activities and polymer molecular weight.

With respect to the polymer properties, narrow dispersities were a feature of all the polymers generated using **Co1**, **Co2**, **Co4** and **Co5** (M_w/M_n range: 1.8–2.7), which implies good control. Moreover, the molecular weights of their polymers (M_w range: 2.9–10.9 kg mol^{-1}) steadily increased in line with the greater steric properties of the *N*-aryl *ortho*-substituents. Indeed, the lower molecular weight polymers generated using **Co1** and **Co4** fall in the range expected for commercially important polyethylene waxes [37]. By contrast, the most hindered 2,6-diisopropyl counterpart, **Co3**, as mentioned earlier, displayed quite different behavior by producing a polymer exhibiting a broad distribution with bimodal characteristics (M_w/M_n = 10.3) and noticeably higher molecular weight (M_w, 75.5 kg mol^{-1}). Certainly, the latter suggests that the bulky *ortho*-isopropyl groups more effectively restrict chain transfer and termination, leading to more effective chain propagation. Notably, when compared to its non-phenyl substituted analogue (**E**$_{2,6\text{-iPr2Ph}}$)$CoCl_2$ (Scheme 1, M_w, 22.75 kg mol^{-1}; M_w/M_n, 1.9) [37], the molecular weight of the polymer produced using **Co3** was significantly higher and the dispersity distinctly broader (Table 2). Though uncertain, when comparing the catalytic behavior of **Co3** with the other cobalt precatalysts (**Co1**, **Co2**, **Co4** and **Co5**), it appears that **Co3** containing the most sterically hindered *ortho*-isopropyl groups is more significantly affected by the presence of potential rotamers [27,38].

To enable a comparison of the current cobalt catalysts with previously reported examples of carbocyclic-fused (**D**)$CoCl_2$ and (**E**)$CoCl_2$ (Scheme 1), Figure 8 collects together their activity, molecular weight and dispersity data and presents this alongside that obtained

using (**G**)$CoCl_2$ (**Co3**); the *N*-aryl group in each case is 2,6-diisopropylphenyl [34–37]. All polymerization catalysts were performed under comparable conditions using MAO as activator at P_{C2H4} as 10 atm.

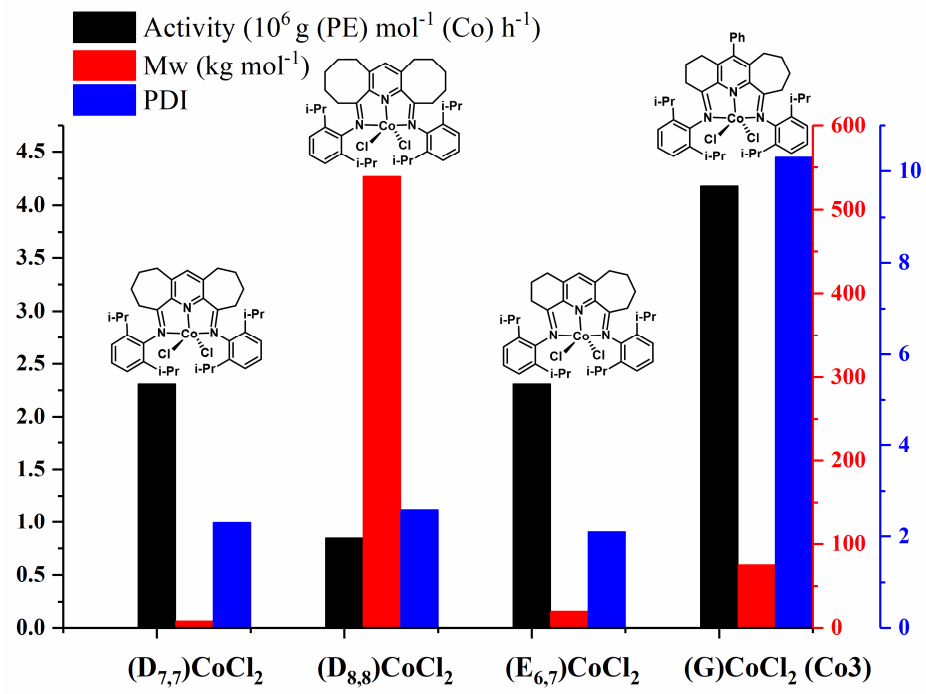

Figure 8. Bar chart comparing catalytic activity and polymer molecular weight/dispersity found for (**G**)$CoCl_2$ (**Co3**) with carbocyclic-fused (**D**$_{7,7}$)$CoCl_2$, (**D**$_{8,8}$)$CoCl_2$ and (**E**$_{6,7}$)$CoCl_2$ (Scheme 1, *N*-aryl = 2,6-*i*-$Pr_2C_6H_3$); all runs were conducted with MAO, P_{C2H4} as 10 atm at 30 or 40 °C.

At first glance, Figure 8 shows that both the ring size of the fused carbocycle and the introduction of a phenyl group to the central pyridine unit can affect the catalytic performance of these cobalt catalysts and their polymer properties. A deeper analysis reveals several key points. First, the molecular weight of the resulting polymers with respect to the cobalt precatalyst declines in the following order: (**D**$_{8,8}$)$CoCl_2$ (n = 3, Scheme 1) > (**G**)$CoCl_2$ (**Co3**) > (**E**$_{6,7}$)$CoCl_2$ > (**D**$_{7,7}$)$CoCl_2$ (n = 2, Scheme 1). This downward trend reflects the steric and flexibility variations of the fused carbocycles and the impact of the *para*-phenyl group incorporation on the relative rates of chain propagation and chain termination [39]. Second, the catalytic activity of this series follows the sequence (**G**)$CoCl_2$ (**Co3**) > (**E**$_{6,7}$)$CoCl_2$ ~ (**D**$_{7,7}$)$CoCl_2$ (n = 2, Scheme 1) > (**D**$_{8,8}$)$CoCl_2$ (n = 3, Scheme 1), suggesting that the combination of the fused six- and seven-membered carbocycles in (**G**)$CoCl_2$ (**Co3**) and (**E**$_{6,7}$)$CoCl_2$ provide the most suitable coordination environment to allow effective chain propagation. Furthermore, the presence of the *para*-phenyl group also positively affects the catalytic activity. It is worth mentioning that six-membered ring (**D**$_{6,6}$)$CoCl_2$ (n = 1, Scheme 1), though not displayed in the figure, was less selective and forms mixtures of low molecular weight polyethylene waxes and α-olefins [34]. In most cases, these fused cobalt precatalysts tend to deliver polymers with narrow polydispersity, with the exception of (**G**)$CoCl_2$ (**Co3**) which produces unusually broad dispersity; an observation that we have tentatively attributed to the rotational isomerism of the *para*-phenyl group and knock-on effect on the number of active species (*vide supra*) [27,38]. Evidently, this observation caused by the appended *para*-phenyl warrants further investigation as it provides an unusual long-range means to influence polymer properties.

2.2.2. Ethylene Polymerization Evaluation Using **Co1**–**Co5** with MMAO as Activator

With MMAO now employed in place of MAO, **Co3** was again utilized as the test precatalyst so as to determine an optimized set of conditions that could be used to screen

the remaining cobalt precatalysts. Once again, the optimization process involved varying the Al:Co molar ratio, run temperature, reaction time and ethylene pressure (Table 3).

Table 3. Ethylene polymerization evaluation using **Co1**–**Co5** with MMAO as activator [a].

Entry	Precat.	Al:Co	T (°C)	t (min)	Activity [b]	M_w [c]	M_w/M_n [c]	T_m (°C) [d]
1	**Co3**	1500	30	30	2.75	66.6	9.6	131.8
2	**Co3**	2000	30	30	3.07	63.6	8.9	131.5
3	**Co3**	2500	30	30	3.24	72.9	9.9	131.9
4	**Co3**	3000	30	30	3.05	71.0	10.2	131.6
5	**Co3**	3500	30	30	2.45	64.4	10.4	131.2
6	**Co3**	2500	20	30	3.56	89.3	5.0	132.8
7	**Co3**	2500	40	30	1.96	44.8	8.5	131.4
8	**Co3**	2500	50	30	1.45	38.5	5.6	131.7
9	**Co3**	2500	60	30	0.80	33.7	5.2	131.1
10	**Co3**	2500	20	5	7.02	66.5	13.5	131.1
11	**Co3**	2500	20	15	5.10	77.0	14.3	131.6
12	**Co3**	2500	20	45	2.40	91.7	15.9	131.5
13	**Co3**	2500	20	60	1.85	97.6	12.7	132.4
14 [e]	**Co3**	2500	20	30	0.53	66.2	8.6	131.5
15 [f]	**Co3**	2500	20	30	2.96	79.5	13.3	131.8
16	**Co1**	2500	20	30	2.75	3.7	2.5	123.9
17	**Co2**	2500	20	30	2.24	13.1	3.3	129.1
18	**Co4**	2500	20	30	2.20	3.8	2.7	124.0
19	**Co5**	2500	20	30	3.03	13.6	3.2	129.7

[a] General conditions: 2.0 µmol of the cobalt precatalyst, MMAO as activator, 100 mL of toluene, 10 atm of ethylene; [b] Values in units of 10^6 g (PE) mol^{-1} (Co) h^{-1}; [c] M_w and M_n in units of kg mol^{-1}, determined via GPC; [d] Determined via DSC; [e] 1 atm of ethylene and 30 mL of toluene; [f] 5 atm of ethylene.

By running **Co3**/MMAO at 30 °C, the optimal Al:Co ratio was identified as 2500:1, leading to a highpoint in activity of 3.24×10^6 g (PE) mol^{-1} (Co) h^{-1} (entry 3 vs. entries 1,2,4,5, Table 3 and Figure S5), which was noticeably less than that seen with the **Co3**/MAO system (Al:Co as 4000:1), highlighting a benefit in terms of cost effectiveness of the reduced amount of activator. By comparison, **Co3**/MAO exhibited a maximum activity of 4.18×10^6 g (PE) mol^{-1} (Co) h^{-1} at a ratio of 4000:1, an observation that reflects the differences in the function of the particular activator. Similarly, at 2500:1, the highest molecular weight polymer of 72.9 kg mol^{-1} was achieved which compares favorably with that seen with **Co3**/MAO. Furthermore, as the ratio is further increased, chain transfer to aluminum starts to become more important, resulting in a perceptible drop in molecular weight. As seen with the **Co3**/MAO runs, the dispersity of the polymers was broad across all molar ratios examined (M_w/M_n range: 8.9–10.4), with a bimodal feature evident in all cases (Figure S5). As noted earlier, we suggest that the origin of this behavior stems from the potential multiple active centers of the catalyst.

Secondly, the temperature of the polymerization using **Co3**/MMAO was progressively increased from 20 °C to 60 °C with the Al:Co molar ratio fixed at 2500:1 (entries 3 and 6–9, Table 3). From the tabulated data, the optimal temperature was 20 °C, with the activity reaching its peak of 3.56×10^6 g (PE) mol^{-1} (Co) h^{-1}, which compares to 30 °C for **Co3**/MAO, reflecting how the nature of the activator can impact on the thermal stability of the catalyst. On the other hand, at 60 °C, the level had declined to only 0.8×10^6 g (PE) mol^{-1} (Co) h^{-1} (Figure S6), as deactivation of the active species had become more important. As for the molecular weight of the polymer, this gradually decreased as temperature increased in accordance with the rate of chain termination becoming more prominent [35,37]. Furthermore, the dispersity narrowed, and the bimodality became less visible in a manner that resembles that seen with **Co3**/MAO. As mentioned earlier, we propose that the higher temperature promotes the favored conformation of the phenyl group, leading to a more uniform active species or to a single chain transfer pathway.

Variation in the run time from 5 min to 60 min, with the temperature kept at 20 °C and the Al:Co molar ratio at 2500:1 (entries 3 and 10–13, Table 3), identified the highest activity of 7.02 × 10^6 g (PE) mol^{-1} (Co) h^{-1} after 5 min. This activity seen after 5 min is notably less than that for **Co3**/MAO, highlighting how variations in the aluminoxane activator can impact on the generation of the active species. By 60 min, the activity had dropped to 1.85 × 10^6 g (PE) mol^{-1} (Co) h^{-1}, in line with gradual deactivation of the active species following a its rapid generation (Figure S7). Inspection of the molecular weight of the polyethylene revealed this to steadily increase over time (from 66.5 kg mol^{-1} to 97.6 kg mol^{-1}), while the dispersity remained broad with bimodal characteristics throughout (M_w/M_n range: 5.0–15.9).

The response of **Co3**/MMAO to variations in pressure was comparable with that seen for **Co3**/MAO, with a reduction in the ethylene pressure from 10 to 5 atm resulting in a slight decrease in both the molecular weight and activity (M_w from 89.3 kg mol^{-1} to 79.5 kg mol^{-1} and activity from 3.56 × 10^6 g (PE) mol^{-1} (Co) h^{-1} to 2.96 × 10^6 g (PE) mol^{-1} (Co) h^{-1}). By comparison, when the pressure was reduced to 1 atm, the decline in activity was more dramatic (M_w to 66.2 kg mol^{-1} and activity to 0.53 × 10^6 g (PE) mol^{-1} (Co) h^{-1}), highlighting the critical pressure required to provide good catalytic performance.

With an operative set of conditions identified using **Co3**/MMAO, these were then utilized to evaluate **Co1**, **Co2**, **Co4** and **Co5** (entries 16–19, Table 3). Examination of the resulting data reveals their values of activity to fall between 2.20 and 3.56 × 10^6 g (PE) mol^{-1} (Co) h^{-1}), which is generally less than that for **Co3**/MAO, and indeed in a narrower range. Nonetheless, the relative level of performance is as follows: **Co3** (2,6-diisopropyl) > **Co5** (2,6-diethyl-4-methyl) > **Co1** (2,6-dimethyl) > **Co2** (2,6-diethyl) > **Co4** (2,4,6-trimethyl) (Figure S8). Compared to the runs performed using MAO, the order was noticeably different, which we presume can be credited to differences in the aluminoxane activator, though the relatively narrow range in values of activity may be a contributing reason. Moreover, this sequence is distinct from what has been reported for related cobalt complexes, in which less steric hindrance generally drives higher activity [35–37].

Nevertheless, the most sterically hindered **Co3**/MMAO affords the highest molecular weight polyethylene (M_w = 89.3 kg mol^{-1}) with the broadest dispersity, which agrees with that observed for **Co3**/MAO and supports the fact that the bulky isopropyl *ortho*-substituents inhibit chain transfer [34,37,57]. On the other hand, **Co1**, **Co2**, **Co4** and **Co5** display better control as is borne out by their narrow dispersities (M_w/M_n range: 2.5–3.3), while their molecular weights are considerably lower (M_w range: = 3.7–13.6 kg mol^{-1}), with the lowest being for *para*-methyl containing **Co1** and **Co4** (M_w = 3.7–3.8 kg mol^{-1}). Overall, the correlation between the polymer type and the precatalyst for the runs using MMAO mirrors that seen with MAO. Furthermore, it highlights the unexpected role played by the *para*-phenyl group, especially with bulkier *N*-aryl *ortho*-substituents whereby multi-site behavior becomes operational, leading to broad dispersities. Notably, the non-phenyl-containing analogue ($\mathbf{E}_{2,6\text{-iPr2Ph}}$)$CoCl_2$ (Scheme 1) under MMAO activation forms lower molecular weight polyethylene (M_w with 19.38 × 10^6 g (PE) mol^{-1} (Co) h^{-1}) and much narrower dispersity (M_w/M_n < 2.1) [37].

2.2.3. Microstructural Analysis of the Polyethylene

On scrutiny of Tables 2 and 3, it is apparent that all polymers display melting points of 122 °C or above, which supports the formation of highly linear polyethylene [35]. To verify this claim and gather some information as to end-group composition, two representative samples prepared using **Co4**/MAO (M_w = 5.66 kg mol^{-1}; entry 19, Table 2) and **Co3**/MMAO (M_w = 89.3 kg mol^{-1}; entry 6, Table 3) were characterized with ^1H and ^{13}C NMR spectroscopy in 1,1,2,2-tetrachloroethane-d_2 at 100 °C.

For the lower molecular weight sample generated using **Co4**/MAO (entry 19, Table 2), an intense single peak around δ 29.44 in the ^{13}C NMR spectrum corresponds to the –$(CH_2CH_2)_n$– repeat unit that confirms the linear nature of the polymer (Figure 9) [35–37]. The lower intensity peaks at δ 31.67 (d), 22.38 (e) and 13.74 (f) can be assigned to an *n*-propyl

group, while the weak downfield peaks at δ 139.00 (b) and 113.85 (a) were characteristic of a terminal vinyl group [2,37,39].

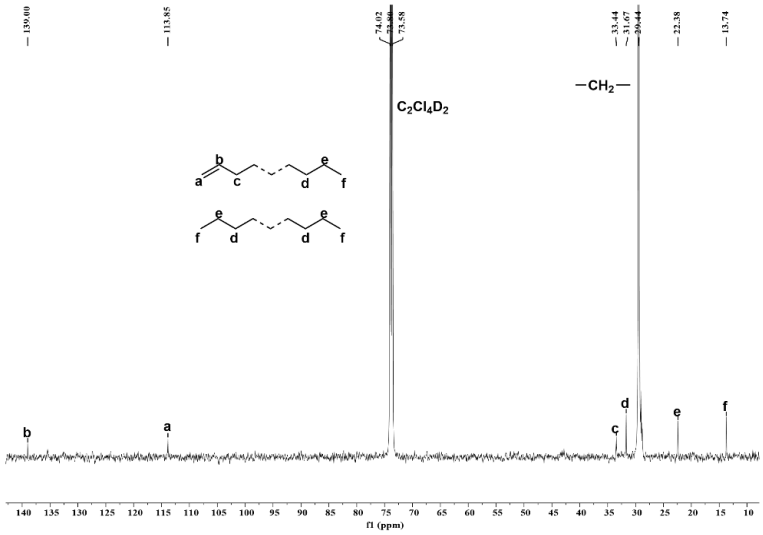

Figure 9. ^{13}C NMR spectrum of the polyethylene obtained using **Co4**/MAO at a run temperature of 30 °C (entry 19, Table 2); recorded in 1,1,2,2-tetrachloroethane-d_2 at 100 °C.

More support for the presence of a vinyl group is provided in the ^{1}H NMR spectrum of this sample (Figure 10), which displays characteristic downfield multiplets around δ 5.86 (H_b) and 5.02 (H_a). Other key signals include the chain end methyl (H_f) that is visible most upfield at δ 0.98. Notably, from the integral ratio of H_b:H_f (1/7.95) (Figure 10), the molar ratio of unsaturated to fully saturated polyethylene can be calculated as 6/5 (see Supporting Information) [30,39,58]. On this basis, *β*-H transfer to the metal or monomer presents the main termination pathway when compared to chain transfer to aluminum (Scheme 3) [2,51,54].

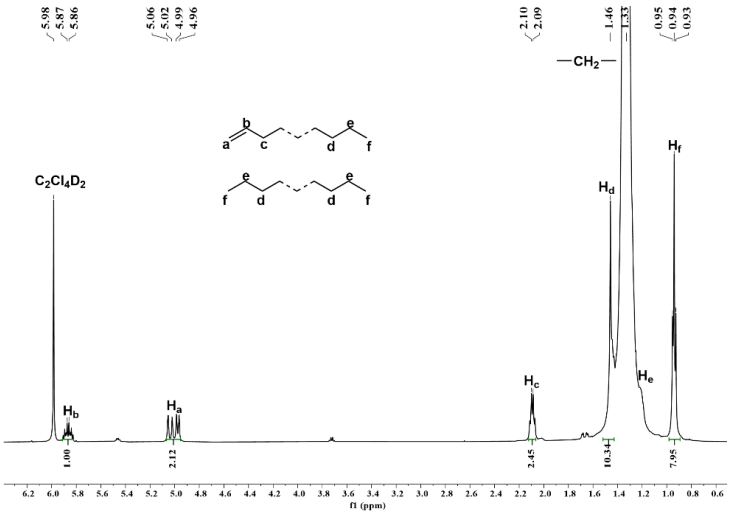

Figure 10. ^{1}H NMR spectrum of the polyethylene obtained using **Co4**/MAO at a run temperature of 30 °C (entry 19, Table 2); recorded in 1,1,2,2-tetrachloroethane-d_2 at 100 °C.

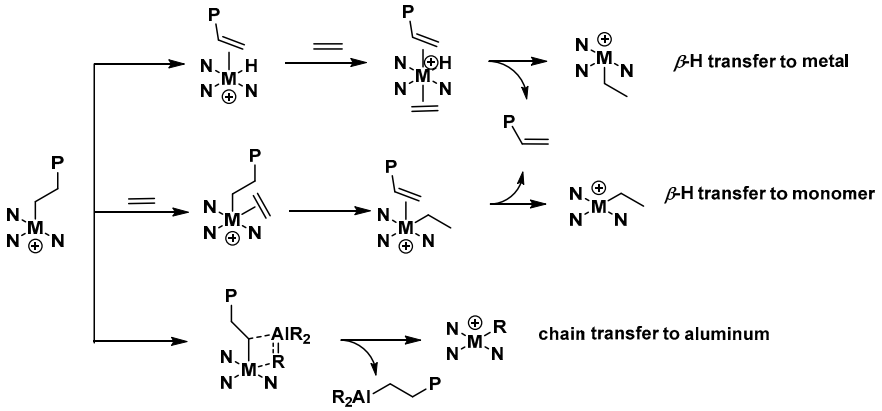

Scheme 3. Potential pathways for the β-H transfer to metal or monomer and chain transfer to aluminum.

By comparison, for the higher molecular weight sample generated using **Co3**/MMAO (entry 6, Table 3), the ^{1}H NMR spectrum similarly showed evidence for unsaturated and fully saturated polymers (Figure S10). However, the molar ratio of unsaturated (vinyl-end) to saturated polyethylene (propyl-end) was quite different, with a value of 4/5 determined (see Supporting Information). According to this finding, chain transfer to aluminum now forms the main pathway rather than the β-H transfer to the metal or the monomer. This finding once again reflects the significant function of an activator on chain transfer pathways.

3. Experimental Section

3.1. General Procedures

Manipulations that required air- and moisture- sensitive compounds were employed under an atmosphere of nitrogen using standard Schlenk techniques or using a nitrogen atmosphere glovebox. Toluene was heated to reflux for more than 12 h over sodium and distilled under a nitrogen atmosphere before use. Isobutyl-modified methylaluminoxane (MMAO, 2.46 M in *n*-heptane, containing 20–25% Al(*i*-Bu)$_3$) and methylaluminoxane (MAO, 1.42 M in toluene) were purchased from Anhui Botai Electronic Materials Co., Chuzhou, China, while high purity ethylene was purchased from Beijing Yansan Petrochemical Co. (Beijing, China) and used as received. Other compounds were purchased from Acros (Geel, Belgium), Aldrich (Saint Louis, MO, USA) or Beijing Chemical Industry Group Co. (Beijing, China). The FT-IR spectra were recorded on a Perkin Elmer System 2000 FT-IR spectrometer (PerkinElmer Scientific, Waltham, MA, USA) at ambient temperature. Elemental analyses were performed on a Flash EA 1112 microanalyzer (Thermo Fisher Scientific, Waltham, MA, USA). Molecular weight (M_w) and dispersity (M_w/M_n) of the polyethylenes were recorded with an Agilent PLGPC 220GPC system (Agilent Technologies Inc., Santa Clara, CA, USA) operating at 150 °C using 1,2,4-trichlorobenzene as eluting solvent. Sample preparation involved dissolving the polyethylenes in 1,2,4-trichlorobenzene at ca. 170 °C for more than 8 h. A Perkin Elmer TA-Q2000 DSC (PerkinElmer Scientific, Waltham, MA, USA) was used to measure the melting points of the polymers under a nitrogen atmosphere. The general procedure was based on 5.0 mg of sample being heated to 160 °C at the rate of 20 °C min^{-1}, then kept for 3 min at 160 °C and cooled to −20 °C at the rate of 20 °C min^{-1}; this was again heated to 160 °C at the rate of 10 °C min^{-1}. The ^{1}H and ^{13}C NMR spectra of the polyethylenes were recorded at 100 °C using a Bruker AVANVE 500 MHz instrument (Bruker Corporation, Billerica, MA, USA). Sample preparation: the polyethylene (about 30 mg) selected for high temperature ^{1}H and ^{13}C NMR spectroscopic measurements was dissolved in 1,1,2,2-tetrachloroethane-d_2 (about 0.6 mL), containing TMS as the internal standard, at 120 °C for more than 2 h before the spectrum was recorded. 11-Phenyl-6,7,8,9,10-pentahydrocyclohepta[*b*]quinoline was prepared according to related procedures [40–42,59].

3.2. Synthesis of 11-phenyl-1,2,3,4,6,7,8,9,10-nonahydrocyclohepta[b]quinoline

This procedure for hydrogenation is based on that reported in the literature [37,43,44]. A stainless steel 250 mL autoclave, equipped with a magnetic stir bar, was charged with 11-phenyl-6,7,8,9,10-penthydrocyclohepta[*b*]quinoline (27.3 g, 0.10 mol), 10% Pd/C (2.7 g) and trifluoroacetic acid (100 mL). The autoclave was evacuated and refilled with hydrogen three times and then maintained at a hydrogen pressure of 40 bar while the reaction was stirred at 80 °C for 16 h. After cooling to ambient temperature, the hydrogen pressure was carefully released, and the reaction mixture filtered. The trifluoroacetic acid was removed using distillation under reduced pressure to give a light green oil. This oil was poured into a saturated aqueous sodium bicarbonate solution (500 mL) which, on vigorous stirring, produced a large amount of white precipitate. Solid sodium bicarbonate was then added, and the pH adjusted to 7. The mixture was then stirred for 1 h and filtered to afford the title compound as a white solid (26.8 g, 96%). ^{1}H NMR (400 MHz, $CDCl_3$): δ 7.42 (dd, *J* = 12.1, 7.3 Hz, 2H), 7.34 (t, *J* = 7.3 Hz, 1H), 7.09–7.02 (m, 2H), 3.06–3.01 (m, 1H), 2.92 (dd, *J* = 10.9, 6.0 Hz, 3H), 2.44–2.39 (m, 1H), 2.33–2.19 (m, 4H), 1.82 (td, *J* = 11.6, 6.1 Hz, 4H), 1.74–1.61 (m, 4H), 1.50–1.43 (m, 1H). ^{13}C NMR (101 MHz, $CDCl_3$): δ 160.32, 153.98, 148.76, 139.17, 133.05, 128.70, 128.50, 128.36, 128.02, 127.35, 127.07, 39.25, 32.96, 32.40, 30.16, 27.88, 27.80, 27.36, 26.79, 23.09.

3.3. Synthesis of 11-phenyl-1,2,3,7,8,9,10-heptahydrocyclohepta[b]quinoline-4,6-dione

Based on that previously reported [37,43,45], the title compound was prepared in two steps. In step 1, a mixture of 11-phenyl-1,2,3,4,6,7,8,9,10-nonahydrocyclohepta[*b*]quinoline (25.0 g, 0.0396 mol) and benzaldehyde (83.0 g, 0.792 mol) in acetic anhydride (71.0 g, 0.693 mol) was stirred at reflux under a nitrogen atmosphere for 72 h (monitored by TLC). After cooling to room temperature, residual acetic anhydride was removed via rotary evaporation. The benzaldehyde was then removed under reduced pressure following the addition of distilled water (100 mL) to give a viscous brown oil. Subsequently, methanol (250 mL) was added, and the mixture was heated to reflux for 0.5 h and then stirred at −30 °C overnight to afford, following filtration, a viscous solid. This crude product was taken up in methanol (100 mL) for 2 h and then filtered to give a yellow powder. Further treatment of this powder with methanol (200 mL) for 2 h followed by filtration gave the pure intermediate compound, 4,6-bis(benzylidene)-11-phenyl-1,2,3,4,6,7,8,9,10-nonahydrocyclohepta[*b*]quinoline, as a yellow powder (31.15 g, 85%).

In the second step, a quantity of 4,6-bis(benzylidene)-11-phenyl-1,2,3,4,6,7,8,9,10-nonahydrocyclohepta[*b*]quinoline (18.0 g, 39.6 mmol) was dissolved in dichloromethane (200 mL) and methanol (600 mL). The solution was treated with a mixture of dry ozone and oxygen at a temperature below −40 °C for 12 h until the solution became totally clear (monitored with TLC). Nitrogen was then bubbled through the mixture for 10 min to remove any residual ozone. Dimethyl sulfide (16 mL) was added, and the temperature of the mixture was slowly raised to room temperature and then left to stir overnight. All volatiles were removed under reduced pressure, affording a dark red oil. To remove the residual benzaldehyde, water (200 mL) was added, and then an azeotropic distillation using rotary evaporation performed and repeated (×8). The resulting yellow suspension was filtered to give the crude product which was recrystallized with ethyl acetate to form pure 11-phenyl-1,2,3,7,8,9,10-heptahydrocyclohepta[*b*]quinoline-4,6-dione as a pale-yellow solid (5.8 g, 48%). ^{1}H NMR (400 MHz, $CDCl_3$): δ 7.63–7.40 (m, 3H, aryl-H), 7.19–7.05 (m, 2H, aryl-H), 2.74 (d, *J* = 12.1 Hz, 4H), 2.64 (s, 2H), 2.58 (s, 2H), 2.04 (s,3H, methylene but ethyl acetate as impurity), 1.91–1.79 (m, 2H), 1.77–167 (m, 2H). ^{13}C NMR (101 MHz, $CDCl_3$): δ 205.78 (C=O), 196.01 (C=O), 156.13 (pyridine-C), 150.58 (pyridine-C), 147.10 (pyridine-C), 140.81 (pyridine-C), 136.11 (pyridine-C), 135.69 (Aryl-C), 129.20 (Aryl-C), 128.15 (Aryl-C), 40.14, 39.41, 28.16, 26.97, 25.16, 22.43, 21.10. FT-IR (cm^{-1}): 2937 (m), 1739 (w), 1698 (s, $\nu_{C=O}$), 1548 (m), 1492 (m), 1442 (m), 1403 (m), 1326 (m), 1218 (m), 1175 (m), 1118(m), 1046 (m), 972 (m), 931 (m), 848 (m), 779 (s), 724 (s), 705 (s), 669 (m).

*3.4. Synthesis of 4,6-di(arylimino)-11-phenyl-1,2,3,7,8,9,10-heptahydrocycloghept[b]quinoline-cobalt(II) Chloride (**Co1**–**Co5**)*

3.4.1. Aryl = 2,6-dimethylphenyl (**Co1**)

A suspension of 11-phenyl-1,2,3,7,8,9,10-heptahydrocyclohepta[*b*]quinoline-4,6-dione (0.153 g, 0.5 mmol), 2,4-dimethylaniline (0.242 g, 2.0 mmol) and $CoCl_2 \cdot 6H_2O$ (0.095 g, 0.4 mmol) in *n*-butanol (10 mL), containing several drops of glacial acetic acid (*ca.* 0.5 mL) as catalyst, was stirred and heated to reflux for about 6 h. On cooling to room temperature, the majority of the acetic acid and *n*-butanol were removed under reduced pressure. Dichloromethane (2 mL) was added to dissolve the residue, and then diethyl ether (30 mL) was introduced to induce precipitation. Following stirring for 10 min, the suspension was allowed to stand, and the supernatant solution was discarded. This process of diethyl ether (30 mL) addition, stirring and discarding of the solution was repeated two more times. The resulting solid was filtered and washed with diethyl ether (3 × 15 mL). The solid was dried at 60 °C to give **Co1** as a brown powder (0.159 g, 62%). FT-IR (cm^{-1}): 2941 (w), 2862 (w), 1671 (w), 1620 (m, $\nu_{C=N}$), 1595 (w), 1564 (m), 1466 (s), 1442 (s), 1374 (m), 1326 (m), 1214 (s), 1164 (m), 1126 (m), 1093 (m), 950 (m), 916 (m), 847 (m), 768 (s), 705 (s). Elemental Analysis: Calcd for $C_{36}H_{37}Cl_2N_3Co$ (641.55) C, 67.40, H, 5.81, N, 6.55. Found: C, 67.13, H, 6.11, N, 6.42%.

3.4.2. Aryl = 2,6-diethylphenyl (**Co2**)

By using the same method as described for **Co1** but with 2,6-diethylaniline as the arylamine, **Co2** was obtained as a brown powder (0.207 g, 74%). FT-IR (cm^{-1}): 2964 (m), 2931 (m), 2872 (m), 1616 (m, $\nu_{C=N}$), 1566 (m), 1447 (s), 1373 (m), 1330 (m), 1215 (s), 1074 (s), 951 (m), 855 (m), 808 (m), 774 (s), 701 (s). Elemental Analysis: Calcd for $C_{40}H_{45}Cl_2N_3Co$ (697.65) C, 68.87, H, 6.50, N, 6.02. Found: C, 68.64, H, 6.71, N, 6.17%.

3.4.3. Aryl = 2,6-diisopropylphenyl (**Co3**)

By using the same method as described for **Co1** but with 2,6-diisopropylaniline as the arylamine, **Co3** was obtained as a brown powder (0.192 g, 64%). FT-IR (cm^{-1}): 2962 (s), 2867 (m), 1616 (m, $\nu_{C=N}$), 1561 (m), 1441 (s), 1383 (m), 1361 (m), 1325 (m), 1250 (s), 1214 (s), 1185 (m), 1051 (s), 943 (m), 853 (m), 804 (m), 773 (s), 707 (s). Elemental Analysis: Calcd for $C_{44}H_{53}Cl_2N_3Co$ (753.76) C, 70.11, H, 7.09, N, 5.57. Found: C, 69.89, H, 7.31, N, 5.38%.

3.4.4. Aryl = 2,4,6-trimethylphenyl (**Co4**)

By using the same method as described for **Co1** but with 2,4,6-trimethylaniline as the arylamine, **Co4** was obtained as a brown powder (0.218 g, 81%). FT-IR (cm^{-1}): 2916 (m), 2863 (m), 1620 (m, $\nu_{C=N}$), 1565 (m), 1476 (s), 1442 (s), 1376 (m), 1325 (m), 1218 (s), 1152 (m), 1075 (m), 1031 (m), 952 (m), 852 (s), 779 (m), 705 (s). Elemental Analysis: Calcd for $C_{38}H_{41}Cl_2N_3Co$ (669.60) C, 68.16, H, 6.17, N, 6.28. Found: C, 67.90, H, 6.52, N, 6.03%.

3.4.5. Aryl = 2,6-diethyl-4-methylphenyl (**Co5**)

By using the same method as described for **Co1** but with 2,6-diethyl-4-methylaniline as the arylamine, **Co5** was obtained as a brown powder (0.207 g, 71%). FT-IR (cm^{-1}): 2964 (m), 2928 (m), 2870 (m), 1614 (m, $\nu_{C=N}$), 1566 (m), 1457 (s), 1374 (m), 1332 (m), 1216 (s), 1150 (m), 1073 (m), 951 (m), 857 (s), 775 (m), 704 (s). Elemental Analysis: Calcd for $C_{42}H_{49}Cl_2N_3Co$ (725.71) C, 69.51, H, 6.81, N, 5.79. Found: C, 69.27, H, 6.98, N, 5.40%.

3.5. Polymerization Study

3.5.1. Ethylene Polymerization at 5 or 10 atm Ethylene Pressure

The higher-pressure polymerization runs were carried out in a stainless-steel autoclave (0.25 L) equipped with a pressure control system, a mechanical stirrer and a temperature controller. The autoclave was first heated to remove any trace amounts of water. Then, a pre-determined amount of cobalt precatalyst was added and the vessel purged using two cycles of pressurization/venting with nitrogen and then pressurized to 3 atm of ethylene to check air tightness. After the required temperature was reached, the ethylene pressure

was decreased to 1 atm and distilled toluene (2 × 25 mL) added with a syringe. The contents were then stirred for 5 min at 400 rpm to ensure dissolution of the precatalyst. The calculated amount of activator (MAO or MMAO) was then added via syringe, followed by additional toluene (2 × 25 mL) to take the total volume of solvent to 100 mL. The ethylene pressure was immediately pressurized to 5 or 10 atm and the mechanical stirring commenced. After the required reaction time, the autoclave was allowed to cool to room temperature and the pressure was slowly released. The contents were quenched with 10% hydrochloric acid in ethanol. The polymer was washed with ethanol, filtered under reduced pressure, dried at 100 °C and then finally weighed.

3.5.2. Ethylene Polymerization at 1 atm Ethylene Pressure

The polymerizations at 1 atm were carried out in a Schlenk vessel. The cobalt complex was added into the vessel and three cycles of pressurization/venting with nitrogen were applied before the vessel was left under an ethylene pressure of 1 atm. Toluene (30 mL) was injected to dissolve the precatalyst and the mixture was stirred and then warmed to the required temperature. The pre-determined amount of activator (MAO or MMAO) was immediately injected with a syringe and the run was commenced. After the required time, the supply of ethylene was stopped, and the vessel was allowed to cool to room temperature. Once the ethylene pressure was released, the mixture was quenched with 10% hydrochloric acid in ethanol. The polyethylene was collected by filtration and then dried at 100 °C before the weight of polymer was recorded.

3.6. X-ray Structure Determinations

Single-crystal X-ray diffraction studies of **Co1**, **Co2** and **Co3** were conducted using an XtaLAB SynergyR single-crystal diffractometer. Cell parameters were obtained by performing the global refinement of the positions of all collected reflections with monochromatic Cu-Kα radiation (λ = 1.54184 Å) at 170(2) K. The intensities were corrected for Lorentz and polarization effects and empirical absorption. The structures were solved using direct methods and refined with full-matrix least-squares on F^2. Non-hydrogen atoms were refined anisotropically. All hydrogen atoms were placed in their calculated positions. Structure solution and refinement were carried out by using the Olex2 1.5 package and SHELXTL [60]. The SQUEEZE option of the crystallographic program PLATON was applied to remove free solvents from the structure of **Co1** [61].

4. Conclusions

In summary, the novel diketone, 11-phenyl-1,2,3,7,8,9,10-heptahydrocyclohepta[*b*]quinoline-4,6-dione (**3**), was successfully synthesized in a multi-step procedure, and then employed in a one-pot method to form cobalt complexes, **Co1**–**Co5**. Besides their characterization via microanalysis and FT-IR spectroscopy, **Co1**, **Co2** and **Co3** were additionally the subject of single X-ray determinations. Upon activation with either MAO or MMAO, all cobalt complexes exhibited high activity (MAO > MMAO) for ethylene polymerization, generating strictly linear polymers, with **Co4**/MAO displaying the highest productivity of 5.66×10^6 g (PE) mol^{-1} (Co) h^{-1} at 30 °C. In terms of the polymer molecular weight, **Co1**, **Co2**, **Co4** and **Co5** had a predilection towards forming low molecular weight polyethylene with narrow dispersity, underlining the good control in place. Conversely, *ortho*-isopropyl **Co3,** under activation with either MAO or MMAO, displayed a preference for forming polyethylenes of not only higher molecular weight but also broad bimodal distributions. Moreover, this distinct behavior for **Co3** is quite different from its non-phenyl substituted comparator ($\mathbf{E}_{2,6\text{-Pr2Ph}}$)$CoCl_2$ (Scheme 1), where the molecular weight is lower and the dispersity significantly narrower [37]. Although uncertain, we believe this multi-site-like behavior displayed by **Co3** derives from the *para*-phenyl group, which can affect the flexibility of the neighboring carbocycles and, in turn, the steric protection of the metal center imparted by the *ortho*-isopropyl substituents. However, it would appear that, for this effect to be operational, the steric properties of the *ortho*-substituents need to exceed that provided

by methyl (**Co1**, **Co4**) and ethyl (**Co2**, **Co5**). This unexpected role of the remote *para*-phenyl group on influencing polymer properties will be the subject of a future investigation. As a final point, end-group analysis of representative polymer samples using ^{1}H and ^{13}C NMR spectroscopy highlights the competition of β-H transfer to the metal or the monomer with chain transfer to aluminum as termination pathways in these polymerizations.

Supplementary Materials: The following supporting information can be downloaded at: https://www.mdpi.com/article/10.3390/catal13101387/s1, Figure S1: ^{1}H NMR spectrum of 11-phenyl-1,2,3,4,6,7,8,9,10-nonahydrocyclohepta[*b*]quinoline (**2**); recorded in $CDCl_3$ (400 MHz); Figure S2: ^{13}C NMR spectrum of 11-phenyl-1,2,3,4,6,7,8,9,10-nonahydrocyclohepta[*b*]quinoline (**2**); recorded in $CDCl_3$ (400 MHz); Figure S3: ^{1}H NMR spectrum of 11-phenyl-1,2,3,7,8,9,10-heptahydrocyclohepta[*b*]quinoline-4,6-dione (**3**); recorded in $CDCl_3$ (400 MHz); Figure S4: ^{13}C NMR spectrum of 11-phenyl-1,2,3,7,8,9,10-heptahydrocyclohepta[b]quinoline-4,6-dione (3); recorded in $CDCl_3$ (400 MHz); Figure S5: (**a**) GPC traces for the polymers produced using **Co3**/MMAO at various Al:Co molar ratios and (**b**) plots of catalytic activity and M_w of the polymers as a function of the Al:Co molar ratio; Figure S6: (**a**) GPC traces for the polymers produced using **Co3**/MMAO at various temperatures and (**b**) plots of catalytic activity and M_w of the polymers as a function of reaction temperature; Figure S7: (**a**) GPC traces for the polymers produced using **Co3**/MMAO at various reaction times and (**b**) plots of catalytic activity and M_w of the polymers as a function of the reaction time; Figure S8: (**a**) GPC traces for the polymers produced using **Co1**–**Co5** with MMAO as activator and (**b**) a bar chart comparing their catalytic activities and polyethylene molecular weight; Figure S9: ^{1}H NMR spectrum of the polyethylene produced using **Co3**/MMAO at a run temperature of 20 °C (entry 6, Table 3); recorded in 1,1,2,2-tetrachloroethane-d_2 at 100 °C; Table S1: Crystal data and structure refinement for **Co1**, **Co2** and **Co3**; CheckCIF/PLATON report for **Co1**, **Co2** and **Co3**.

Author Contributions: Conceptualization, W.-H.S.; methodology, Y.W. and Z.W.; software, Y.W., Y.M. and W.Z.; validation, Y.W., S.Z. and Q.Z; formal analysis, Y.W.; investigation, Y.W. and Z.W G.A.S.; resources, W.-H.S.; data curation, Y.W.; writing—original draft preparation, Y.W.; writing—review and editing, Y.W., G.A.S., Q.Z. and W.-H.S.; visualization, W.Z. and W.-H.S.; supervision, W.-H.S.; project administration, W.-H.S.; funding acquisition, W.-H.S. All authors have read and agreed to the published version of the manuscript.

Funding: This research was funded by the National Natural Science Foundation of China (21871275).

Data Availability Statement: The data presented in this study are available in this article.

Acknowledgments: Z.W. thanks the support from the Nature Science Foundation of Hebei Province (B2022204020) and Talent Introduction Foundation of Hebei Agricultural University (YJ201931). Research Project of Fundamental Scientific Research Business Expenses of Provincial Colleges and Universities in Hebei Province (KY2021028); Opening Fund of CAS Key Laboratory of Engineering Plastics, Institute of Chemistry. G.A.S. thanks the Chinese Academy of Sciences for a President's International Fellowship for Visiting Scientists.

Conflicts of Interest: The authors declare no conflict of interest.

References

1. Bianchini, C.; Giambastiani, G.; Luconi, L.; Meli, A. Olefin oligomerization, homopolymerization and copolymerization by late transition metals supported by (imino)pyridine ligands. *Coord. Chem. Rev.* **2010**, *254*, 431–455. [CrossRef]
2. Wang, Z.; Solan, G.A.; Zhang, W.; Sun, W.-H. Carbocyclic-fused *N,N,N*-pincer ligands as ring-strain adjustable supports for iron and cobalt catalysts in ethylene oligo-/polymerization. *Coord. Chem. Rev.* **2018**, *363*, 92–108. [CrossRef]
3. Wang, Z.; Mahmood, Q.; Zhang, W.; Sun, W.-H. Recent progress on the tridentate iron complex catalysts for ethylene oligo-/polymerization. In *Advances in Organometallic Chemistry*; Pérez, P.J., Ed.; Academic Press: Cambridge, MA, USA, 2023; Volume 79, pp. 41–86.
4. Chirik, P.J. Carbon-Carbon Bond Formation in a Weak Ligand Field: Leveraging Open-Shell First-Row Transition-Metal Catalysts. *Angew. Chem. Int. Ed.* **2017**, *56*, 5170–5181. [CrossRef]
5. Humphries, M.J.; Tellmann, K.P.; Gibson, V.C.; White, A.J.P.; Williams, D.J. Investigations into the Mechanism of Activation and Initiation of Ethylene Polymerization by Bis(imino)pyridine Cobalt Catalysts: Synthesis, Structures, and Deuterium Labeling Studies. *Organometallics* **2005**, *24*, 2039–2050. [CrossRef]
6. Sun, W.-H. Novel Polyethylenes via Late Transition Metal Complex Pre-catalysts. In *Polyolefins: 50 years after Ziegler and Natta II: Polyolefins by Metallocenes and Other Single-Site Catalysts*; Kaminsky, W., Ed.; Springer: Berlin/Heidelberg, Germany, 2013; pp. 163–178.

7. Champouret, Y.; Hashmi, O.H.; Visseaux, M. Discrete iron-based complexes: Applications in homogeneous coordination-insertion polymerization catalysis. *Coord. Chem. Rev.* **2019**, *390*, 127–170. [CrossRef]
8. Small, B.L.; Brookhart, M.; Bennett, A.M.A. Highly Active Iron and Cobalt Catalysts for the Polymerization of Ethylene. *J. Am. Chem. Soc.* **1998**, *120*, 4049–4050. [CrossRef]
9. Britovsek, G.J.P.; Gibson, V.C.; McTavish, S.J.; Solan, G.A.; White, A.J.P.; Williams, D.J.; Britovsek, G.J.P.; Kimberley, B.S.; Maddox, P.J. Novel olefin polymerization catalysts based on iron and cobalt. *Chem. Commun.* **1998**, 849–850. [CrossRef]
10. Gibson, V.C.; Redshaw, C.; Solan, G.A. Bis(imino)pyridines: Surprisingly Reactive Ligands and a Gateway to New Families of Catalysts. *Chem. Rev.* **2007**, *107*, 1745–1776. [CrossRef]
11. Ma, J.; Feng, C.; Wang, S.L.; Zhao, K.Q.; Sun, W.-H.; Redshaw, C.; Solan, G.A. Bi- and tri-dentate imino-based iron and cobalt pre-catalysts for ethylene oligo-/polymerization. *Inorg. Chem. Front.* **2014**, *1*, 14–34. [CrossRef]
12. Sun, W.-H.; Jie, S.; Zhang, S.; Zhang, W.; Song, Y.; Ma, H. Iron Complexes Bearing 2-Imino-1,10-phenanthrolinyl Ligands as Highly Active Catalysts for Ethylene Oligomerization. *Organometallics* **2006**, *25*, 666–677. [CrossRef]
13. Jie, S.; Zhang, S.; Wedeking, K.; Zhang, W.; Ma, H.; Lu, X.; Deng, Y.; Sun, W.-H. Cobalt(II) complexes bearing 2-imino-1,10-phenanthroline ligands: Synthesis, characterization and ethylene oligomerization. *C. R. Chim.* **2006**, *9*, 1500–1509. [CrossRef]
14. Pelletier, J.D.A.; Champouret, Y.D.M.; Cadarso, J.; Clowes, L.; Gañete, M.; Singh, K.; Thanarajasingham, V.; Solan, G.A. Electronically variable imino-phenanthrolinyl-cobalt complexes; synthesis, structures and ethylene oligomerisation studies. *J. Organomet. Chem.* **2006**, *691*, 4114–4123. [CrossRef]
15. Jie, S.; Zhang, S.; Sun, W.-H.; Kuang, X.; Liu, T.; Guo, J. Iron(II) complexes ligated by 2-imino-1,10-phenanthrolines: Preparation and catalytic behavior toward ethylene oligomerization. *J. Mol. Catal. A Chem.* **2007**, *269*, 85–96. [CrossRef]
16. Jie, S.; Zhang, S.; Sun, W.-H. 2-Arylimino-9-phenyl-1,10-phenanthrolinyl-iron, -cobalt and -nickel Complexes: Synthesis, Characterization and Ethylene Oligomerization Behavior. *Eur. J. Inorg. Chem.* **2007**, *2007*, 5584–5598. [CrossRef]
17. Sun, W.-H.; Kong, S.; Chai, W.; Shiono, T.; Redshaw, C.; Hu, X.; Guo, C.; Hao, X. 2-(1-(Arylimino)ethyl)-8-arylimino-5,6,7-trihydroquinolylcobalt dichloride: Synthesis and polyethylene wax formation. *Appl. Catal. A-Gen.* **2012**, *447–448*, 67–73. [CrossRef]
18. Zhang, W.; Chai, W.; Sun, W.-H.; Hu, X.; Redshaw, C.; Hao, X. 2-(1-(Arylimino)ethyl)-8-arylimino-5,6,7-trihydroquinoline Iron(II) Chloride Complexes: Synthesis, Characterization, and Ethylene Polymerization Behavior. *Organometallics* **2012**, *31*, 5039–5048. [CrossRef]
19. Britovsek, G.J.P.; Baugh, S.P.D.; Hoarau, O.; Gibson, V.C.; Wass, D.F.; White, A.J.P.; Williams, D.J. The role of bulky substituents in the polymerization of ethylene using late transition metal catalysts: A comparative study of nickel and iron catalyst systems. *Inorg. Chim. Acta* **2003**, *345*, 279–291. [CrossRef]
20. Zabel, D.; Schubert, A.; Wolmershäuser, G.; Jones, R.L.; Thiel, W.R. Iron and Cobalt Complexes of Tridentate N-Donor Ligands in Ethylene Polymerization: Efficient Shielding of the Active Sites by Simple Phenyl Groups. *Eur. J. Inorg. Chem.* **2008**, *2008*, 3648–3654. [CrossRef]
21. Abu-Surrah, A.S.; Lappalainen, K.; Repo, T.; Piironen, U.; Leskela, M. New bis(imino)pyridine-iron(II)- and cobalt(II)-based catalysts: Synthesis, characterization and activity towards polymerization of ethylene. *J. Organomet. Chem.* **2002**, *648*, 55–61. [CrossRef]
22. Wang, S.; Li, B.; Liang, T.; Redshaw, C.; Li, Y.; Sun, W.-H. Synthesis, characterization and catalytic behavior toward ethylene of 2-[1-(4,6-dimethyl-2-benzhydrylphenylimino)ethyl]-6-[1-(arylimino)ethyl]pyridylmetal (iron or cobalt) chlorides. *Dalton Trans.* **2013**, *42*, 9188–9197. [CrossRef]
23. Yu, J.; Huang, W.; Wang, L.; Redshaw, C.; Sun, W.-H. 2-[1-(2,6-Dibenzhydryl-4-methylphenylimino)ethyl]-6-[1-(arylimino)ethyl]pyridylcobalt(II) dichlorides: Synthesis, characterization and ethylene polymerization behavior. *Dalton Trans.* **2011**, *40*, 10209–10214. [CrossRef] [PubMed]
24. He, F.; Zhao, W.; Cao, X.-P.; Liang, T.; Redshaw, C.; Sun, W.-H. 2-[1-(2,6-dibenzhydryl-4-chlorophenylimino)ethyl]-6-[1-aryliminoethyl]pyridyl cobalt dichlorides: Synthesis, characterization and ethylene polymerization behavior. *J. Organomet. Chem.* **2012**, *713*, 209–216. [CrossRef]
25. Mahmood, Q.; Ma, Y.; Hao, X.; Sun, W.-H. Substantially enhancing the catalytic performance of bis(imino)pyridylcobaltous chloride pre-catalysts adorned with benzhydryl and nitro groups for ethylene polymerization. *Appl. Organomet. Chem.* **2019**, *33*, e4857. [CrossRef]
26. Bariashir, C.; Zhang, R.; Vignesh, A.; Ma, Y.; Liang, T.; Sun, W.-H. Enhancing Ethylene Polymerization of NNN-Cobalt(II) Precatalysts Adorned with a Fluoro-substituent. *ACS Omega* **2021**, *6*, 4448–4460. [CrossRef] [PubMed]
27. Zhang, Q.; Li, Z.; Han, M.; Xiang, J.; Solan, G.A.; Ma, Y.; Liang, T.; Sun, W.-H. Fluorinated cobalt catalysts and their use in forming narrowly dispersed polyethylene waxes of high linearity and incorporating vinyl functionality. *Catal. Sci. Technol.* **2021**, *11*, 656–670. [CrossRef]
28. Liu, T.; Liu, M.; Ma, Y.; Solan, G.A.; Liang, T.; Sun, W.-H. Cobalt Catalysts Bearing ortho-(4,4′-Dichlorobenzhydryl) Substituents and Their Use in Generating Narrowly Dispersed Polyethylene of High Linearity. *Eur. J. Inorg. Chem.* **2022**, *2022*, e202200396. [CrossRef]
29. Liu, M.; Jiang, S.; Ma, Y.; Solan, G.A.; Sun, Y.; Sun, W.-H. CF_3O-Functionalized Bis(arylimino)pyridine–Cobalt Ethylene Polymerization Catalysts: Harnessing Solvent Effects on Performance and Polymer Properties. *Organometallics* **2022**, *41*, 3237–3248. [CrossRef]

30. Han, M.; Oleynik, I.I.; Liu, M.; Ma, Y.; Oleynik, I.V.; Solan, G.A.; Liang, T.; Sun, W.-H. Ring size enlargement in an ortho -cycloalkyl-substituted bis(imino)pyridine-cobalt ethylene polymerization catalyst and its impact on performance and polymer properties. *Appl. Organomet. Chem.* **2021**, *36*, e6529. [CrossRef]
31. Ba, J.; Du, S.; Yue, E.; Hu, X.; Flisak, Z.; Sun, W.-H. Constrained formation of 2-(1-(arylimino)ethyl)-7-arylimino-6,6-dimethylcyclopentapyridines and their cobalt(II) chloride complexes: Synthesis, characterization and ethylene polymerization. *RSC Adv.* **2015**, *5*, 32720–32729. [CrossRef]
32. Huang, F.; Zhang, W.; Yue, E.; Liang, T.; Hu, X.; Sun, W.-H. Controlling the molecular weights of polyethylene waxes using the highly active precatalysts of 2-(1-aryliminoethyl)-9-arylimino-5,6,7,8-tetrahydrocycloheptapyridylcobalt chlorides: Synthesis, characterization, and catalytic behavior. *Dalton Trans.* **2016**, *45*, 657–666. [CrossRef]
33. Guo, J.; Wang, Z.; Zhang, W.; Oleynik, I.I.; Vignesh, A.; Oleynik, I.V.; Hu, X.; Sun, Y.; Sun, W.-H. Highly Linear Polyethylenes Achieved Using Thermo-Stable and Efficient Cobalt Precatalysts Bearing Carbocyclic-Fused NNN-Pincer Ligand. *Molecules* **2019**, *24*, 1176. [CrossRef] [PubMed]
34. Appukuttan, V.K.; Liu, Y.; Son, B.C.; Ha, C.-S.; Suh, H.; Kim, I. Iron and Cobalt Complexes of 2,3,7,8-Tetrahydroacridine-4,5(1H,6H)-diimine Sterically Modulated by Substituted Aryl Rings for the Selective Oligomerization to Polymerization of Ethylene. *Organometallics* **2011**, *30*, 2285–2294. [CrossRef]
35. Du, S.; Zhang, W.; Yue, E.; Huang, F.; Liang, T.; Sun, W.-H. α,α′-Bis(arylimino)-2,3:5,6-bis(pentamethylene)pyridylcobalt Chlorides: Synthesis, Characterization, and Ethylene Polymerization Behavior. *Eur. J. Inorg. Chem.* **2016**, *2016*, 1748–1755. [CrossRef]
36. Wang, Z.; Solan, G.A.; Mahmood, Q.; Liu, Q.; Ma, Y.; Hao, X.; Sun, W.-H. Bis(imino)pyridines Incorporating Doubly Fused Eight-Membered Rings as Conformationally Flexible Supports for Cobalt Ethylene Polymerization Catalysts. *Organometallics* **2018**, *37*, 380–389. [CrossRef]
37. Wang, Z.; Ma, Y.; Guo, J.; Liu, Q.; Solan, G.A.; Liang, T.; Sun, W.-H. Bis(imino)pyridines fused with 6- and 7-membered carbocylic rings as *N,N,N*-scaffolds for cobalt ethylene polymerization catalysts. *Dalton Trans.* **2019**, *48*, 2582–2591. [CrossRef] [PubMed]
38. Cámpora, J.; Naz, A.M.; Palma, P.; Rodríguez-Delgado, A.; Álvarez, E.; Tritto, I.; Boggioni, L. Iron and Cobalt Complexes of 4-Alkyl-2,6-diiminopyridine Ligands: Synthesis and Ethylene Polymerization Catalysis. *Eur. J. Inorg. Chem.* **2008**, *2008*, 1871–1879. [CrossRef]
39. Zhang, Q.; Wu, N.; Xiang, J.; Solan, G.A.; Suo, H.; Ma, Y.; Liang, T.; Sun, W.-H. Bis-cycloheptyl-fused bis(imino)pyridine-cobalt catalysts for PE wax formation: Positive effects of fluoride substitution on catalytic performance and thermal stability. *Dalton Trans.* **2020**, *49*, 9425–9437. [CrossRef]
40. Rajendran, S.; Sivalingam, K.; Karnam Jayarampillai, R.P.; Wang, W.L.; Salas, C.O. Friedländer's synthesis of quinolines as a pivotal step in the development of bioactive heterocyclic derivatives in the current era of medicinal chemistry. *Chem. Biol. Drug. Des.* **2022**, *100*, 1042–1085. [CrossRef]
41. Dabiri, M.; Baghbanzadeh, M.; Nikcheh, M.S. Oxalic Acid: An Efficient and Cost-Effective Organic Catalyst for the Friedländer Quinoline Synthesis under Solvent-Free Conditions. *Monatsh. Chem.* **2007**, *138*, 1249–1252. [CrossRef]
42. Wang, Z.; Lin, Q.; Ma, N.; Liu, S.; Han, M.; Yan, X.; Liu, Q.; Solan, G.A.; Sun, W.-H. Direct synthesis of ring-fused quinolines and pyridines catalyzed by NN_HY-ligated manganese complexes (Y = NR_2 or SR). *Catal. Sci. Technol.* **2021**, *11*, 8026–8036. [CrossRef]
43. Bell, T.W.; Khasanov, A.B.; Drew, M.G.B. Role of Pyridine Hydrogen-Bonding Sites in Recognition of Basic Amino Acid Side Chains. *J. Am. Chem. Soc.* **2002**, *124*, 14092–14103. [CrossRef] [PubMed]
44. Vierhapper, F.W.; Eliel, E.L. Selective Hydrogenation of Quinoline and Its Homologs, Isoquinoline, and Phenyl-Substituted Pyridines in the Benzene Ring. *J. Org. Chem.* **1975**, *40*, 2729–2734. [CrossRef]
45. Thummel, R.P.; Lefoulon, F.; Cantu, D.; Mahadevan, R. Polyaza Cavity-Shaped Molecules. Annelated Derivatives of 2- (2'-Py ridyl)-1,8-naphthyridine and 2,2'-Bi-1,8-naphthyridine. *J. Org. Chem.* **1984**, *49*, 2208–2212. [CrossRef]
46. Addison, A.W.; Rao, T.N. Synthesis, structure, and spectroscopic properties of copper(II) compounds containing nitrogen–sulphur donor ligands; the crystal and molecular structure of aqua [1,7-bis(N-methylbenzimidazol-2′-yl)-2,6-dithiaheptane]copper(II) perchlorate. *J. Chem. Soc. Dalton Trans.* **1984**, 1349–1356. [CrossRef]
47. Seitz, M.; Milius, W.; Alt, H.G. Iron(II) coordination compounds with ω-alkenyl substituted bis(imino)pyridine ligands: Self-immobilizing catalysts for the polymerization of ethylene. *J. Mol. Catal. A Chem.* **2007**, *261*, 246–253. [CrossRef]
48. Pelascini, F.; Wesolek, M.; Peruch, F.; Lutz, P.J. Modified Pyridine-Bis(imine) Iron and Cobalt Complexes: Synthesis, Structure, and Ethylene Polymerization Study. *Eur. J. Inorg. Chem.* **2006**, *2006*, 4309–4316. [CrossRef]
49. Huang, F.; Zhang, W.; Sun, Y.; Hu, X.; Solan, G.A.; Sun, W.-H. Thermally stable and highly active cobalt precatalysts for vinyl-polyethylenes with narrow polydispersities: Integrating fused-ring and imino-carbon protection into ligand design. *New J. Chem.* **2016**, *40*, 8012–8023. [CrossRef]
50. Wu, J.; Pan, Q.; Rempel, G.L. Solubility of ethylene in toluene and toluene/styrene–butadiene rubber solutions. *J. Appl. Polym. Sci.* **2005**, *96*, 645–649. [CrossRef]
51. Gibson, V.C.; Solan, G.A. Olefin Oligomerizations and Polymerizations Catalyzed by Iron and Cobalt Complexes Bearing Bis(imino)pyridine Ligands. In *Catalysis without Precious Metals*; Bullock, R.M., Ed.; Wiley-VCH: Weinheim, Germany, 2010; pp. 111–141.
52. Gibson, V.C.; Solan, G.A. Iron-Based and Cobalt-Based Olefin Polymerisation Catalysts. In *Metal Catalysts in Olefin Polymerization*; Guan, Z., Ed.; Springer: Berlin/Heidelberg, Germany, 2009; pp. 107–158.
53. Small, B.L.; Brookhart, M. Iron-Based Catalysts with Exceptionally High Activities and Selectivities for Oligomerization of Ethylene to Linear α-Olefins. *J. Am. Chem. Soc.* **1998**, *120*, 7143–7144. [CrossRef]

54. Britovsek, G.J.P.; Mastroianni, S.; Solan, G.A.; Baugh, S.P.D.; Redshaw, C.; Gibson, V.C.; White, A.J.P.; Williams, D.J.; Elsegood, M.R.J. Oligomerisation of Ethylene by Bis(imino)pyridyliron and -cobalt Complexes. *Chem. Eur. J.* **2000**, *6*, 2221–2231. [CrossRef]
55. Ittel, S.D.; Johnson, L.K.; Brookhart, M. Late-Metal Catalysts for Ethylene Homo- and Copolymerization. *Chem. Rev.* **2000**, *100*, 1169–1204. [CrossRef] [PubMed]
56. Zhai, F.; Jordan, R.F. (α-Diimine)nickel Complexes That Contain Menthyl Substituents: Synthesis, Conformational Behavior, and Olefin Polymerization Catalysis. *Organometallics* **2017**, *36*, 2784–2799. [CrossRef]
57. Britovsek, G.J.P.; Bruce, M.; Gibson, V.C.; Kimberley, B.S.; Maddox, P.J.; Mastroianni, S.; McTavish, S.J.; Redshaw, C.; Solan, G.A.; Stromberg, S.; et al. Iron and Cobalt Ethylene Polymerization Catalysts Bearing 2,6-Bis(Imino)Pyridyl Ligands: Synthesis, Structures, and Polymerization Studies. *J. Am. Chem. Soc.* **1999**, *121*, 8728–8740. [CrossRef]
58. Zhang, Q.; Zuo, Z.; Ma, Y.; Liang, T.; Yang, X.; Sun, W.-H. Fluorinated 2,6-bis(arylimino)pyridyl iron complexes targeting bimodal dispersive polyethylenes: Probing chain termination pathways via a combined experimental and DFT study. *Dalton Trans.* **2022**, *51*, 8290–8302. [CrossRef] [PubMed]
59. Pan, B.; Liu, B.; Yue, E.; Liu, Q.; Yang, X.; Wang, Z.; Sun, W.-H. A Ruthenium Catalyst with Unprecedented Effectiveness for the Coupling Cyclization of γ-Amino Alcohols and Secondary Alcohols. *ACS Catal.* **2016**, *6*, 1247–1253. [CrossRef]
60. Sheldrick, G. SHELXT—Integrated space-group and crystal-structure determination. *Acta Crystallogr. A* **2015**, *71*, 3–8. [CrossRef]
61. Sheldrick, G.M. Crystal structure refinement with SHELXL. *Acta Crystallogr. C* **2015**, *71*, 3–8. [CrossRef]